metals

MDPI

Article

Effect of Temperature and Solidification Structure Evolution of S355 Slabs with Different Corner Shapes on Transverse Corner Cracks

Minglin Wang [1,2,*], Hui Zhang [1,2,*], Heping Liu [3] and Lijun Xu [1,2]

[1] National Engineering & Research Center of Continuous Casting Technology, Central Iron and Steel Research Institute, Beijing 100081, China
[2] Zhongda National Engineering & Research Center of Continuous Casting Technology Co., Ltd., Beijing 100081, China
[3] Material Digital R&D Center, China Iron & Steel Research Institute Group, Beijing 100081, China
* Correspondence: wangminglin2005@sina.com (M.W.); zhangh@cisri.com.cn (H.Z.); Tel.: +86-10-62182665 (M.W.); +86-10-62187142 (H.Z.)

Abstract: The evolution process of corner temperatures for a typical micro-alloyed steel S355 is numerically simulated under various working conditions. The microstructure near the corner cracks of the S355 slab is experimentally examined, and the austenite/ferrite transformation temperatures of S355 steel during heating and cooling are measured. The results indicate that the right-angle slab corner temperature at the exit of the mould rapidly decreased to below Ar_3 under intensive cooling in the foot roller zone. The film-like ferrite began to precipitate along the austenite grain boundary at the slab corner. The transformation from ferrite to austenite cannot be fully realized because the corner temperature cannot be quickly returned to Ac_3 or higher. The slab transverse corner cracks occur along the film-like ferrite during the bending process. The chamfered slab, which modifies the original right angle of the slab into the 30° chamfered angle with a chamfered length of 60 mm, can significantly weaken the heat transfer and cooling effect of the slab corner. The chamfered slab corner temperature always remained above Ar_3 during the bending and straightening processes. Precipitation of the pro-eutectoid film-like ferrite along the grain boundary cannot occur during cooling for the chamfered slab. The chamfered slab can keep the corner temperature above Ar3 and effectively avoid the occurrence of transverse corner cracks caused by grain boundary embrittlement.

Keywords: transverse corner crack; micro-alloyed steel; film-like ferrite; phase transformation temperature; chamfered mould

Citation: Wang, M.; Zhang, H.; Liu, H.; Xu, L. Effect of Temperature and Solidification Structure Evolution of S355 Slabs with Different Corner Shapes on Transverse Corner Cracks. *Metals* **2022**, *12*, 1383. https://doi.org/10.3390/met12081383

Academic Editor: Francesca Borgioli

Received: 10 June 2022
Accepted: 16 August 2022
Published: 20 August 2022

1. Introduction

Transverse corner crack defects of the slab are common in the continuous casting production of micro-alloyed steel in major steel companies worldwide [1–3]. The existence of transverse corner cracks not only increases the production cost, but also reduces the production efficiency, making the slab impossible to realize the hot delivery and hot charging, which is a key point that affects the smoothness of the cast-rolling interface.

Over the years, extensive research on the control method of the defects in continuous casting of steel have been performed [4–7]. In the existing technology, several control methods are generally used. The first method is to optimize the secondary cooling water system, reasonably reducing the amount of secondary cooling water, increasing the corner temperature of the slab, and avoiding the third brittle zone of the slab during bending and straightening [8–10]. Secondly, using the method of rapid cooling and reheating at the slab corner, the slab corner temperature is quickly reduced to below Ar_1 (i.e., the ending temperature of austenite to ferrite transformation during cooling), and thereafter returned to the temperature above Ac_3 (i.e., the ending temperature of ferrite to austenite

transformation during heating). On the basis of the phase transformation for the purpose of refining the grain, the second phase precipitation of particles, such as Nb(CN) and Ti(CN), on the pre-eutectoid ferrite film, improved the high-temperature toughness of the steel [11–15]. Finally, using chamfered mould technology to reduce the cooling effect of the slab corner and increase the temperature of the slab corner concurrently improved the stress state of the slab corner and effectively prevented the occurrence of transverse corner cracks in the slab [16–20].

However, in actual production, transverse cracks at the corners of the cast slab not only occur at the corners, but also usually appear at a distance of 5 to 15 mm from the corners. The micro-alloying elements such as Nb, V, and Ti in S355 steel are precipitated in carbonitrides during the continuous casting process, which deteriorates the hot ductility of the steel. The transverse corner cracks are prone to occur during the bending and straightening process of the S355 slab. Some transverse cracks occur on the wide face and narrow face by passing through the corners, and some are near the corner on the wide face.

In this study, the morphology and microstructure of transverse corner cracks of S355 slab are observed. The austenite and ferrite transformation temperatures of S355 steel during heating and cooling are measured, and the causes of the cracks are analyzed. The temperature of right-angle and chamfered slab near the corner area under weak and intensive cooling conditions in the foot roller zone during the bending and straightening process are investigated by numerical simulation. Combining the structure of the cracks of the slab and morphology characteristics by the Gleeble experiment, the causes of the transverse cracks near the corner area are analyzed. The effect of the chamfered mould technology on the slab transverse corner cracks is clarified.

2. Materials and Methods

2.1. Experimental Materials and Methods

The chemical composition of S355 in this experiment is shown in Table 1. A 500 mm-long specimen is cut from industrial slab with corner transverse cracks. The corner of the slab is pickled by hydrochloric acid for observing the morphology of the corner transverse cracks. Then, the corner specimen with a transverse crack is sectioned along the vertical direction, smoothed on the sandpapers, polished with polishing paste, and then etched by 4% nitric acid in ethanol for observing the microstructure near the crack.

Table 1. Chemical composition of typical steel (wt%).

Steel	C	Si	Mn	S	P	Als	N	Ti	Nb	V
S355	0.17	0.29	1.51	0.002	0.017	0.037	0.003	0.012	0.017	0.051

The specimen for measuring the phase transition temperature is cut by wire cutting along the width direction of the slab and processed into cylindrical samples with a diameter of 5 mm and a length of 3 mm. Differential scanning calorimetry (DSC) is used to measure the phase transition temperatures of the S355 steel.

Tensile tests are performed on a Gleeble 1500D thermal stress/strain simulator (DS Inc., Poestenkill, NY, USA). The specimens are taken from an S355 slab, and are cut away from the center. The size of the specimen is 10 mm in diameter and 110 mm in length, with M10 threads at the two ends. The specific size is shown in Figure 1.

The schematic diagram of the tensile test process is shown in Figure 2. The temperature range of the high-temperature tensile test is 650 °C to 1000 °C, and the high-temperature tensile test is measured at intervals of 50 °C. After the specimen is broken by stretching, it is subjected to water quenching. The specimen is smoothed with sandpaper, and then polished with polishing paste. Finally, 4% nitric acid in ethanol is used for etching, and the fracture structure is observed with optical microscopy.

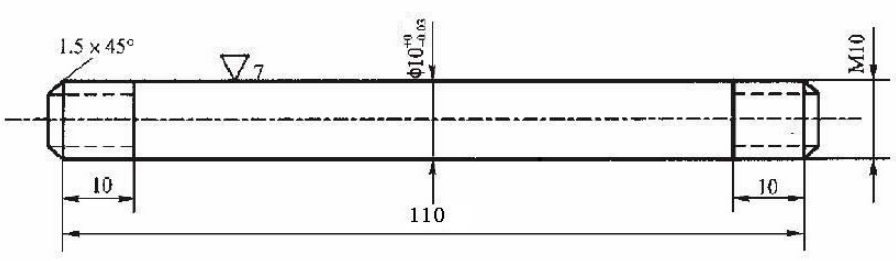

Figure 1. Dimensions (mm) of high-temperature tensile specimens.

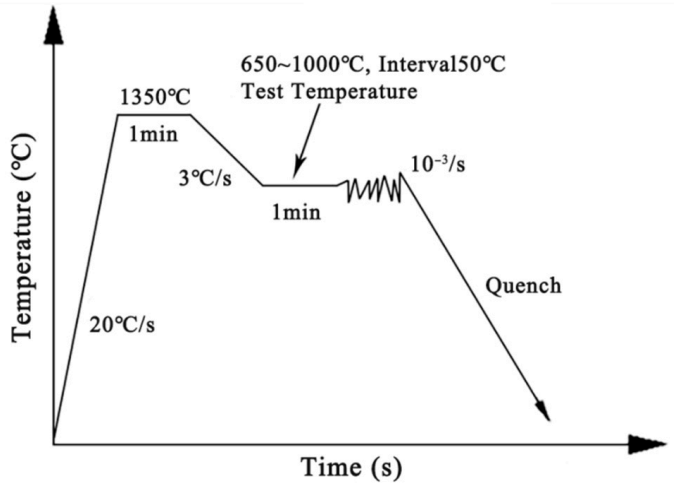

Figure 2. Schematic diagram of the tensile test process.

2.2. Numerical Simuation Methods

In this study, a numerical analysis of heat transfer and solidification in the continuous casting of an S355 steel slab are preformed to predict the effect of the temperature profiles near the corner area on the possible occurrence of transverse corner crack defects by using a two-dimensional solidification model with the concept of effective heat conductivity [21–24]. Compared with the complex coupled model of fluid flow, heat transfer, and solidification in continuous casting of steel, it is simpler for the on-line thermal tracking and spraying control of the strand. In this model, it is assumed that the finite 2D slice of the slab being considered moves with the strand at a velocity equal to the casting speed. The influence of fluid turbulence and convection on heat transfer are taken into account by increasing the thermal conductivity of steel in the liquid pool region [22–24]. Neglecting the heat conductivity along the axial direction, in a rectangular Cartesian coordinate system, the equation based on the concept of effective heat conductivity model in continuous casting can be expressed as:

$$\rho V_c \frac{\partial h}{\partial z} = \frac{\partial}{\partial x}\left(k_{eff}\frac{\partial T}{\partial x}\right) + \frac{\partial}{\partial y}\left(k_{eff}\frac{\partial T}{\partial y}\right) + S_T \quad (1)$$

where ρ is the density (kg·m^{-3}), V_c is the casting speed (m·s^{-1}), h is the enthalpy, k_{eff} is the effective heat conductivity (W·m^{-1}·K^{-1}), T is the temperature (K), z is the distance away from the meniscus (m), x, y is the slab width (m) and thickness direction (m), respectively, and S_T is the latent heat term.

$$S_T = \rho V_c \Delta H_f \frac{\partial f_s}{\partial z} \quad (2)$$

where ΔH_f is the latent heat of solidification (J·kg^{-1}), f_s is the solidus fraction, $V_c = z/t$ and t is the time (s).

In the mould cooling zone, the local heat convection boundary along the height of the mould is used, which is validated by the average heat flux through the mould walls, calculated from the mould's actual water flow (Q_w) and the rise in temperature of the cooling water (ΔT_w):

$$\overline{q} = \rho_w Q_w C_{p,w} \Delta T_w \quad (3)$$

where ρ_w is the density and $C_{p,w}$ is the specific heat of the cooling water.

Beyond the mould zone, a convective heat transfer boundary condition depending on the spraying water volume in every segment is imposed [24], and the overall heat transfer coefficient is determined from the cooling water's volume flow rate and the radiative heat transfer by:

$$q_s = h_s(T_s - T_w) + \sigma\varepsilon({T_s}^4 - {T_\infty}^4) \quad (4)$$

where h_s is the heat transfer coefficient, T_s is the slab surface temperature (K), σ is the Stefan Boltzman constant and ε is the emissivity of the slab surface, T_w and T_∞ are the cooling water and the surrounding temperatures (K), respectively.

In the radiation cooling zone below sprays, the surface heat flux can be represented via the following expression:

$$q_s = \sigma\varepsilon({T_s}^4 - {T_\infty}^4) \quad (5)$$

Due to the symmetry in the square section of slab, only a quadrant of its cross-section is considered for the numerical analysis. The symmetric boundary condition through the center line is:

$$q_s = 0 \quad (6)$$

The above governing equations associated with the boundary conditions are solved numerically using a finite control volume method. The initial temperature during unsteady casting is supposed to be the incoming temperature of molten steel.

Figure 3 shows the specified geometry and non-uniform hexahedral mesh system for the S355 slab with the transverse size of 250 mm $\times$ 1600 mm. A conventional slab caster with right-angle mould for S355 production at the casting speed of 1.0 m/min is used as a reference to a chamfered slab caster with a chambered angle of $\alpha = 30^\circ$ and the chamfered length of $L = 60$ mm. Two spraying cooling conditions including an intensive cooling and a weak cooling in the foot roller are examined. The temperature evolutions of the monitored points (labeled in Figure 3) in the slab are focused to analyze the effect of the varying cooling conditions on the transverse corner cracks.

The characteristic temperatures at key solidification lengths are discussed. The effective cooling length in the mould is S = 0.80 m away from the meniscus. The length at the foot roller ending is 1.5 m. The length at the beginning of bending is S = 2.52 m. The length at the beginning of straightening is S = 17.16 m, and the length at the end of straightening is S = 19.2 m. A schematic drawing of key characteristic positions for discussion is shown in Figure 4. Other geometrical parameters and computational conditions of the slab caster are given in Table 2. The thermal-physical properties of the S355 steel used in this study are listed in Table 3.

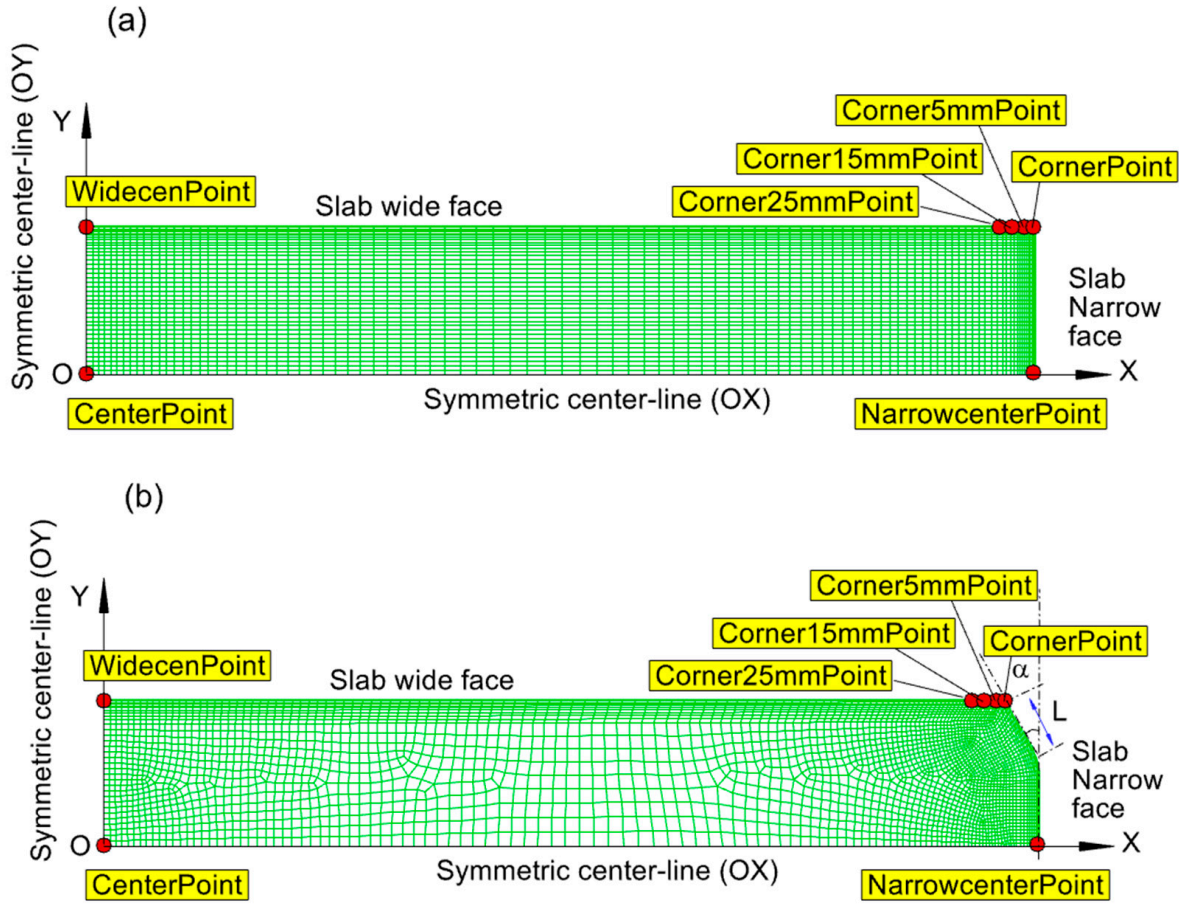

Figure 3. Geometry, mesh system and monitoring points for: (**a**) conventional slab ($\alpha = 0°$, $L = 0$ mm); (**b**) chamfered slab ($\alpha = 30°$, $L = 60$ mm).

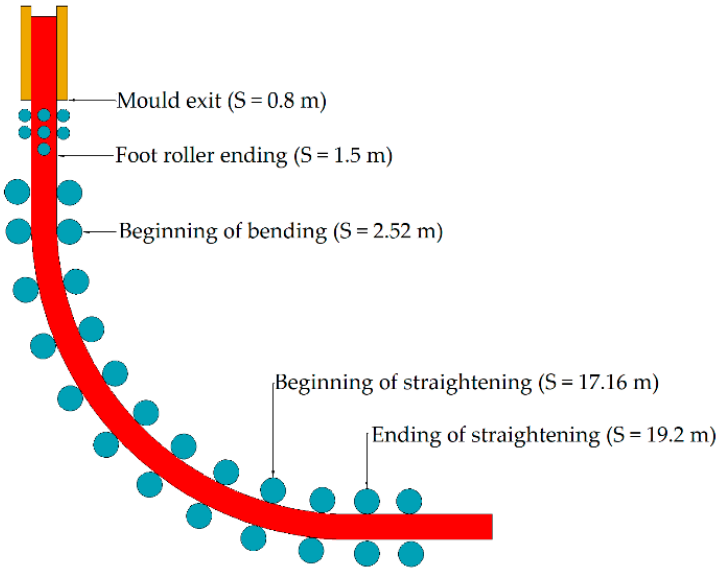

Figure 4. Schematic drawing of key characteristic positions.

Table 2. Thermophysical properties of S355 steel used in the study.

Parameter	Value
Density of steel(kg·m^{-3})	7020
Latent heat of steel (J ·kg^{-1})	2.72×10^5
Specific heat (J·kg^{-1}·K^{-1})	711
Thermal conductivity (W·m^{-1}·K^{-1})	$12.5 + 0.01108 \times T$
Liquidus temperature (K)	1790
Solidus temperature (K)	1728

Table 3. Casting process parameters adopted in the simulation.

Parameter	Value
Slab transverse section size (mm × mm)	1600 (Length) × 250 (Thickness)
Effective mould length (m)	0.80
Initial casting temperature (K)	1815
Casting speed(m·min^{-1})	1.0
Spraying cooling segment lengthof slab wide face (m)	0.49, 0.87, 1.061, 1.64, 1.951, 3.906, 5.790
Spraying water flow rate of slab wide face (L·min^{-1})	451, 610, 211, 254,2 38, 326, 255
Spraying cooling length in the foot roller zone (m)	0.70
Spraying water flow rate for an intensive cooling in the foot roller zone (L·min^{-1})	150
Spraying water flow rate for a weak cooling in the foot roller zone (L·min^{-1})	72
Cooling water temperature (K)	300
Cooling water flow rate in the mould (m^3·h^{-1})	420
Averaged water temperature rising in mould (°C)	6.0

3. Results and Discussion

3.1. Crack Morphology of Typical Micro-Alloyed Steel S355 Slab

Figure 5 shows the morphology of the transverse corner cracks in a typical micro-alloyed steel of a right-angle slab. Some cracks are in the corners (Figure 5a), and some cracks are 5–15 mm away from the corners (Figure 5b). The microstructure of the area near the crack is shown in Figure 5. It can be observed that the microstructure of the typical micro-alloyed steel S355 slab is in the vicinity of the transverse corner cracks, which mainly consists of two parts: the pro-eutectoid film-like ferrite generated along the grain boundary and the acicular ferrite in the grain (see Figure 6a). The transverse corner cracks of the slab are all formed in the middle of the ferrite film along the grain boundaries. The enlarged crack morphology is shown in Figure 6b.

Form Figure 6, it can be deduced that the crack characteristics are as follows: (1) the cracks are all formed in the middle of the film-like ferrite along the grain boundary, indicating that when cracks occur, the slab corner begins to undergo $\gamma \rightarrow \alpha$ transformation, i.e., the temperature in the corner area drops below Ar_3 (i.e., the starting temperature of austenite-to-ferrite transformation during cooling); and (2) the pre-eutectoid film-like ferrite generated along the grain boundary caused grain boundary embrittlement, which is the internal cause of the slab transverse corner cracks during the bending and straightening processes. Therefore, reasonably increasing the slab corner temperature by a weak cooling to control it above Ar_3 is an effective method in avoiding the occurrence of transverse corner cracks on the micro-alloyed steel slab.

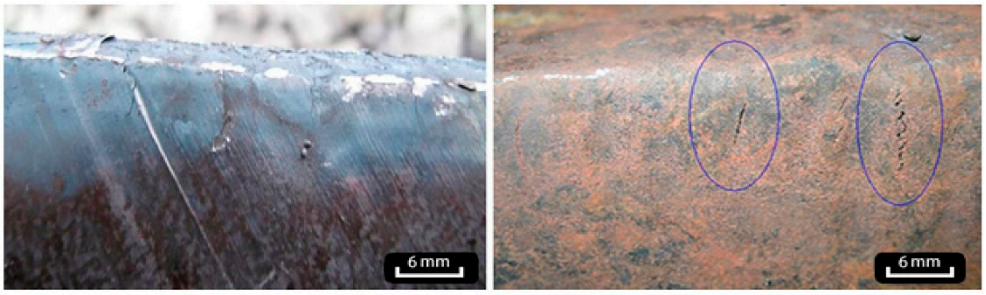

Figure 5. Transverse corner cracks in a typical micro-alloyed steel of a right-angle slab. (**a**) Transverse corner cracks; (**b**) cracks at a distance of 5–15 mm from the corners.

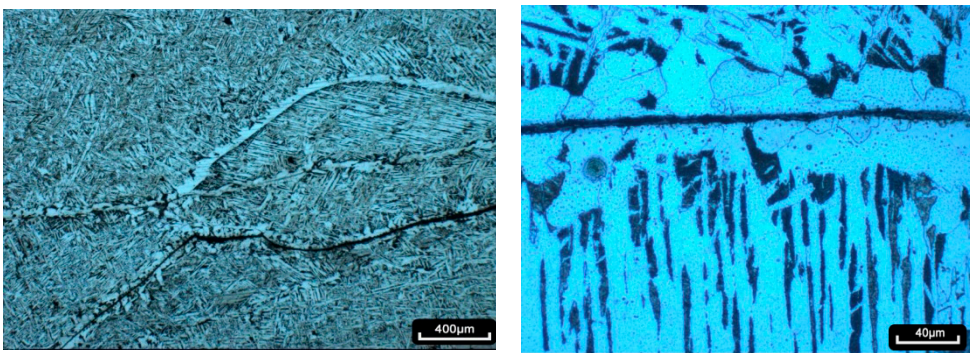

Figure 6. Microstructure of the crack. (**a**) Pro-eutectoid ferrite film generated along the grain boundary; (**b**) enlarged crack morphology.

3.2. Phase-Transformation Temperature

Figure 7 shows the phase transformation temperatures measured by DSC differential analyser during cooling and heating of S355. The analysis shows that Ac_1 (i.e., the starting temperature of ferrite-to-austenite transformation during heating), Ac_3, Ar_1, and Ar_3 are 736.5 °C, 852.6 °C, 646.0 °C, and 797.0 °C, respectively.

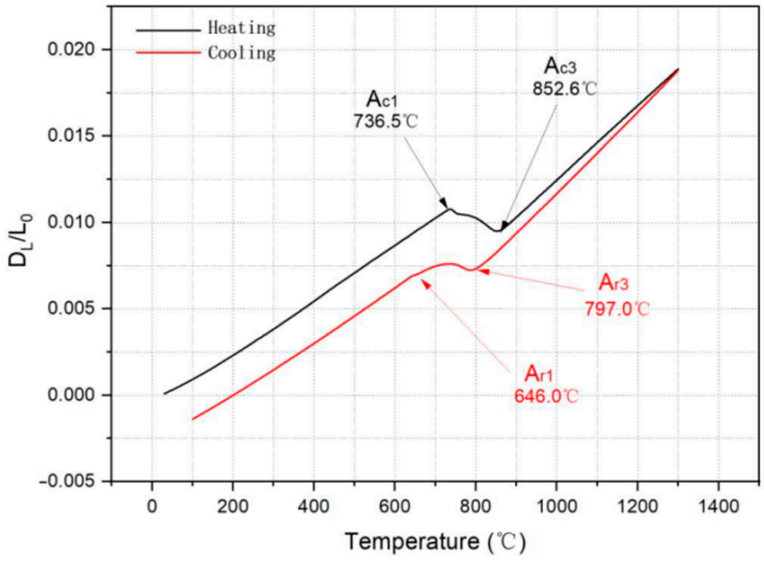

Figure 7. Measured phase transformation temperature of S355 steel.

3.3. Tensile Test Results

3.3.1. Hot Ductility and Tensile Strength

Figure 8 shows the hot ductility(RA) and tensile strength(σb) of S355 at different temperature tested by the Gleeble 1500D thermal stress/strain simulator. It can be seen that the tensile strength increases with the decrease in temperature during the continuous cooling process of the sample. The tensile strength is 49 MPa when the test temperature is 1000 °C. When the temperature decreases to 650 °C, the tensile strength increased to 179 MPa. However, the hot ductility first decreases and then increases with the decrease in temperature. The lowest hot ductility is only 18% at 750 °C, and the hot ductility trough is in the 670 °C~850 °C temperature range of the S355. Therefore, the cracks are prone to occur when bending or straightening in this embrittlement zone.

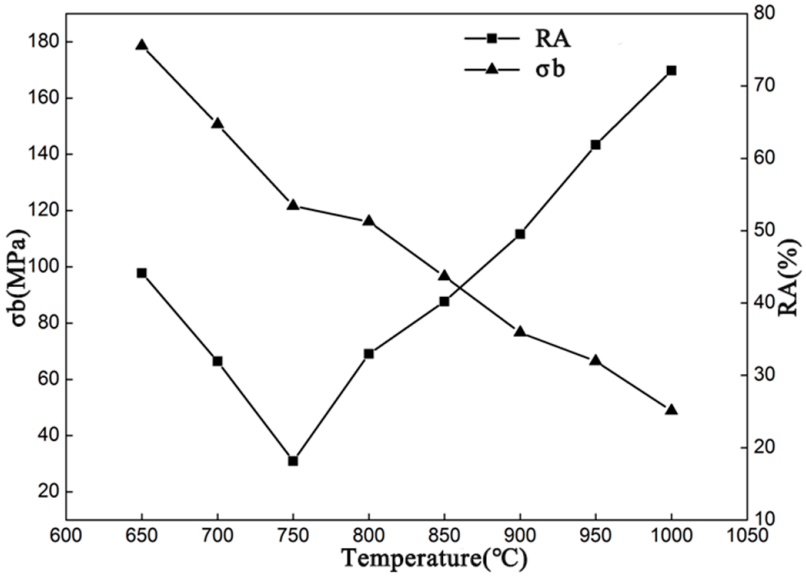

Figure 8. Measured hot ductility and tensile strength of S355 steel.

3.3.2. Microstructure

The tensile fracture microstructure of the S355 slab is shown in Figure 9. It can be observed that when the test temperature is 850 °C, the room-temperature structure is mainly martensite, thereby indicating that the structure of the sample at a high temperature is austenite. When the sample is cooled to 800 °C, there is a small amount of discontinuous pre-eutectoid ferrite at the grain boundaries at room temperature, and continuous pre-eutectoid ferrite is formed when the sample is cooled to 750 °C. The existence of this continuous ferrite film results in the grain boundary embrittlement, which became the original source of cracks. The temperature of the microstructure also corresponds to the trough of the hot ductility of the sample. The amount of ferrite precipitation increases, the ferrite film becomes thicker, and the ferrite begins to precipitate inside the grains at 700 °C. When the test temperature is further reduced to 650 °C, in addition to the thick ferrite film already formed at the grain boundaries, a large amount of ferrite is formed inside the grains. Combined with Figure 6, it can be further proved that, in actual production, the corner cracks occur when the slab temperature is below the Ar_3.

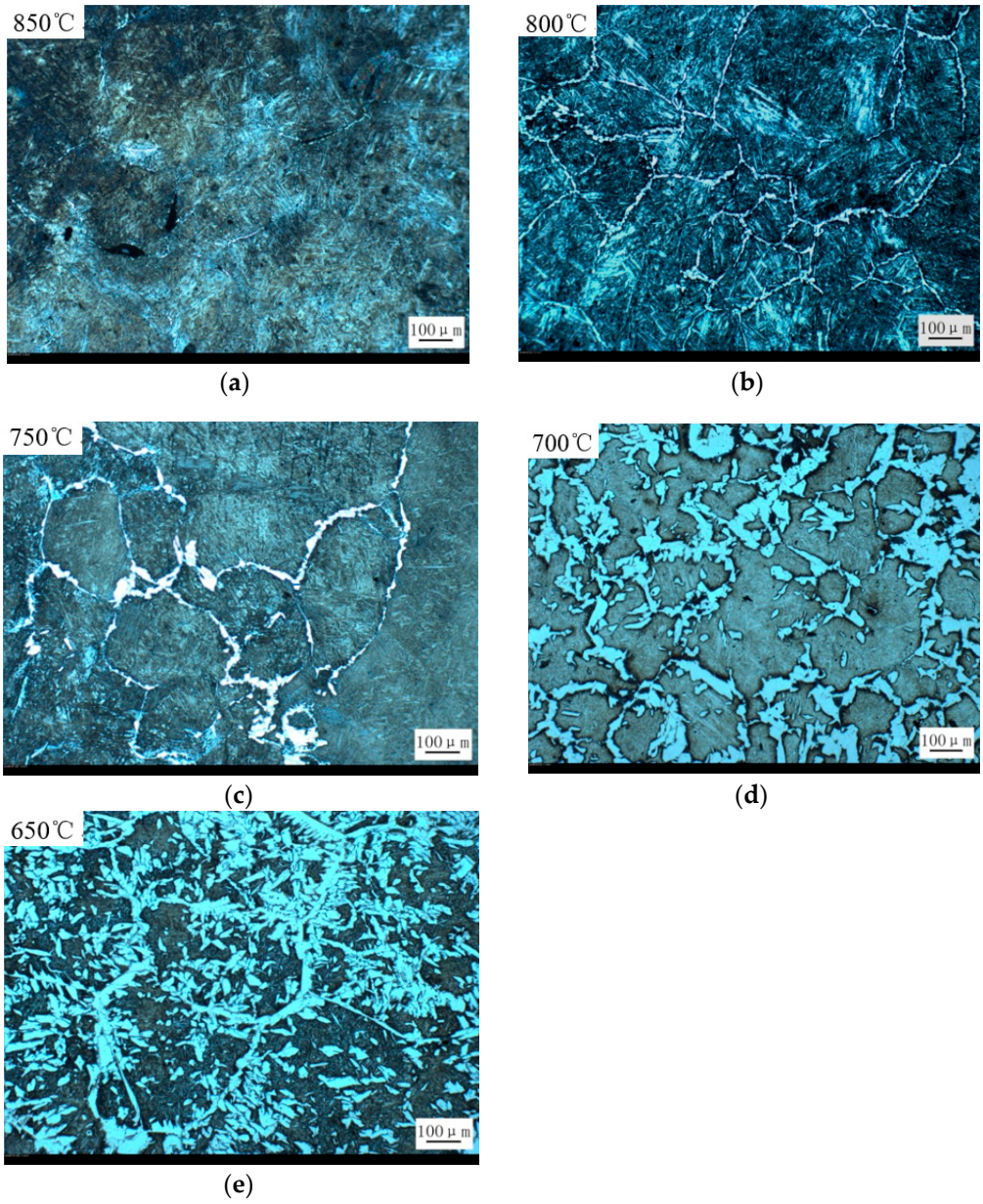

Figure 9. Fracture microstructures from the tensile test at different temperatures. (**a**) 850 °C, (**b**) 800 °C, (**c**) 750 °C, (**d**) 700 °C, (**e**) 650 °C.

3.4. Simulation of Corner Temperature in Continuous Casting Slabs with Different Corner Shapes

3.4.1. Temperature Characteristics of the Right-Angle Slab Corner

Figure 10 shows the predicted temperature profiles at the monitored points (labeled in Figure 3a) along the casting direction for the right-angle slab under an intensive cooling condition in the foot roller zone. It can be seen that the temperature of the slab center (CenterPoint) presents the slowest cooling and gives a final solidification core length of about 23 m (Figure 10a). There is a rapid temperature drop on the corner (CornerPoint). An enlarged view of the temperature distribution from the mould to the bending segment in Figure 10b shows that even at a small distance of 5 mm away from the corner point (Center5mmPoint)along the wide face, there is an obvious change in the temperature. The minimum temperature values at the CornerPoint and Corner5mmPoint at the end of foot roller (S = 1.5 m) under the intensive cooling are 575 °C and 646 °C, respectively. With the increase in the distance from the meniscus, the temperature at the CornerPoint and Corner5mmPoint can gradually increase.

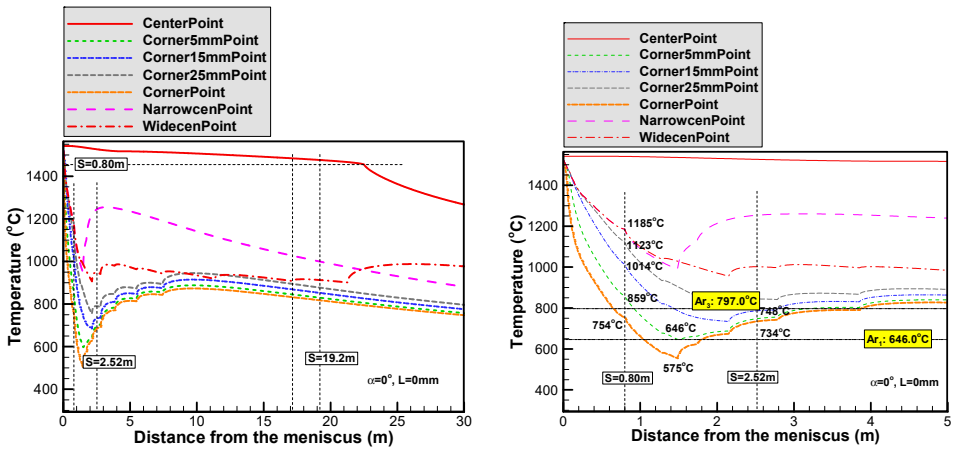

Figure 10. Temperature distribution under intensive cooling in foot roller zone of the right-angle slab. (**a**) The whole process of slab solidification, (**b**) enlarged view of mould and bending section.

Table 4 lists the detailed temperature values at the distances of 0 mm, 5 mm, 15 mm, and 25 mm along the wide face of the right-angle slab of the S355 steel at the selected characteristic positions, including the mould exit, the end of the foot roller, the beginning of the bending, and the beginning and end of the straitening segment. If an intensive cooling process is adopted, the temperature at the position of 5 mm from the slab corner can be reduced to 646 °C at the foot roller ending (S = 1.5 m), which is in the pure ferrite phase. Although the temperatures can rise up to 748 °C, it is still below the measured temperature of the Ac_3 point (852.6 °C) of S355 steel. Therefore, the slab cannot obtain a pure austenite phase; when the slab begins to bend (S = 2.52 m) at this situation, the cracks are prone to occur during the bending process. The temperature at the position of 15 mm from the slab corner is 785 °C at the foot roller ending (S = 1.5 m), which is higher than Ar_1. At this time, the microstructure is in the austenite and ferrite two-phase region, rather than pure ferrite region. The temperature is 787 °C at the beginning of bending (S = 2.52 m), the film-like ferrite phase still exists, and cracks are easy to generate during the bending process. The temperature at the Corner25mmPoint is 844 °C, which is in the austenite region at the beginning of bending.

Table 4. Temperature of right-angle slab under intensive cooling (°C).

Right-Angle Slab	CornerPoint	Corner5mmPoint	Corner15mmPoint	Corner25mmPoint
Mould exit (S = 0.8 m)	754	859	1014	1123
Foot roller ending (S = 1.5 m)	575	646	785	902
Beginning of bending (S = 2.52 m)	734	748	787	844
Beginning of straightening (S = 17.16 m)	834	847	871	897
Ending of straightening (S = 19.2 m)	820	832	855	880

As a comparison to Figure 10, Figure 11 shows the temperature distribution on the same monitored points of the right-angle slab under the weak cooling condition in the foot-roller zone. The temperatures at the corner point and its nearby area are different from those in the intensive cooling. The minimum temperature at the slab corner is 754 °C at the exit of the mould and can return to 840 °C during the bending process (S = 2.52 m), which is close to the temperature of Ac_3 of S355 steel. However, at a distance of 5 mm from the slab corner, the temperature is maintained above 797 °C of Ar_3, and no ferrite film can be formed. It is still in the hot ductility trough of S355, and the possibility of bending cracks still exists.

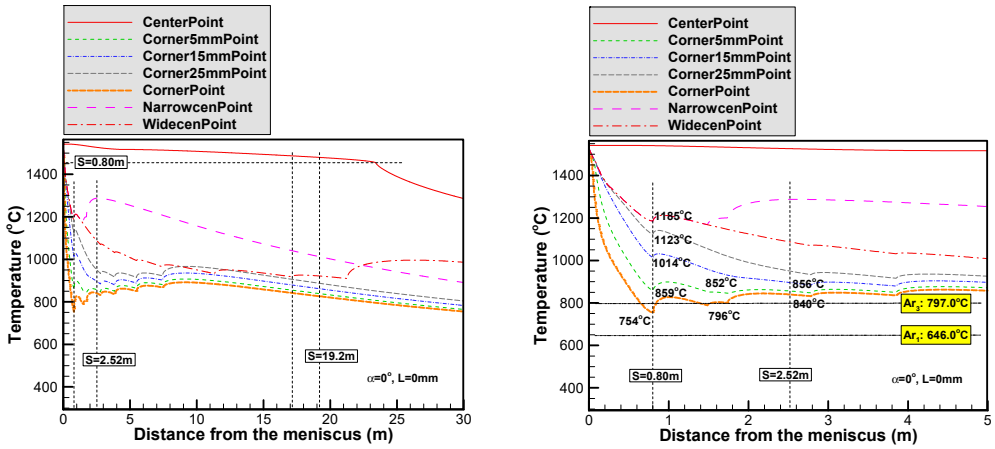

Figure 11. Temperature distribution under weak cooling in foot roller zone of the right-angle slab. (**a**) The whole process of slab solidification, (**b**) enlarged view of mould and bending section.

As shown in Tables 4 and 5, the temperature at the beginning of straightening for the CornerPoint and Corner5mmPoint are 834 °C and 842 °C, respectively. Both are kept above 797 °C for Ar_3 of S355 steel, which could effectively prevent the occurrence of ferrite films during the straightening process. However, the temperatures are still in the embrittlement zone. Therefore, the straightening cracks cannot be avoided for the right-angle slab with an intensive cooling or a weak cooling.

Table 5. Temperature of right-angle slab under weak cooling (°C).

Right-Angle Slab	CornerPoint	Corner5mmPoint	Corner15mmPoint	Corner25mmPoint
Mould exit (S = 0.8 m)	754	859	1014	1123
Foot roller ending (S = 1.5 m)	796	852	957	1053
Beginning of bending (S = 2.52 m)	840	856	896	950.1
Beginning of straightening (S = 17.16 m)	842	855	879	906
Ending of straightening (S = 19.2 m)	826	839	862	887

3.4.2. Temperature Characteristics of Chamfered Slab Corners

Figures 12 and 13 show the predicted temperature profiles at the monitored points (labeled in Figure 3b) along the casting direction for the chamfered slab ($\alpha = 30°$, $L = 60$ mm) with an intensive cooling and weak cooling in the foot roller zone, respectively. Table 6 lists the temperature values at each characteristic position of the chamfered slab. Under the same cooling conditions, the chamfered slab corner temperature is higher than that of the right-angle slab. At the beginning of the bending (S = 2.52 m), it is found that the corner temperatures of the wide-face of the chamfered slab are 929 °C and 1016.2 °C for the intensive cooling and the weak cooling, respectively, which are higher than the temperature of Ac_3 of S355 steel. This confirms that no ferrite film is formed in the slab corner area during the bending process, and bending cracks can be avoided.

At the beginning of the straightening process (S = 17.16 m), the corner temperatures of the wide face of the chamfered slab under the intensive and weak cooling processes are 910 °C and 917 °C, which are 76 °C and 75 °C higher than those of the right-angle slab, respectively. The higher temperature at the corner can effectively avoid the embrittlement zone of the slab and thus prevent the occurrence of straightening cracks. Therefore, it can be concluded that the chamfered slab can be favorable for avoiding the occurrence of transverse corner cracks, whether the intensive cooling or the weak cooling in the foot roller zone are used.

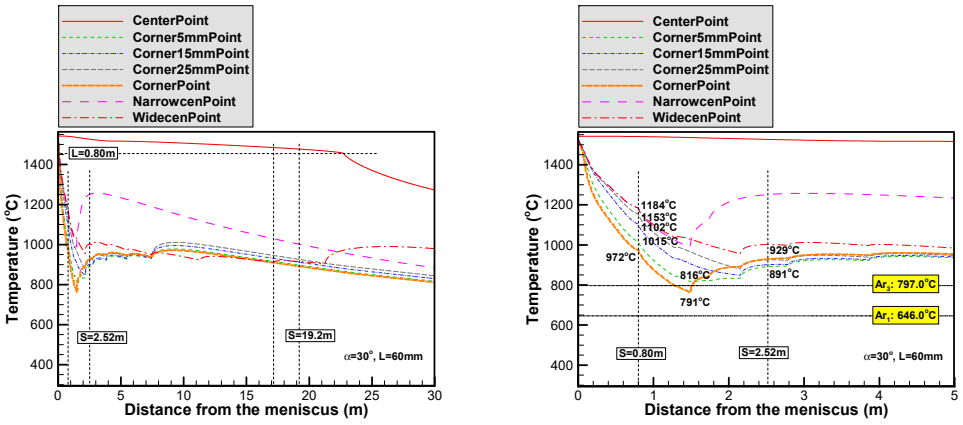

(**a**) (**b**)

Figure 12. Temperature distribution under intensive cooling in foot roller zone of the chamfered slab. (**a**) The whole process of slab solidification, (**b**) enlarged view of mould and bending section.

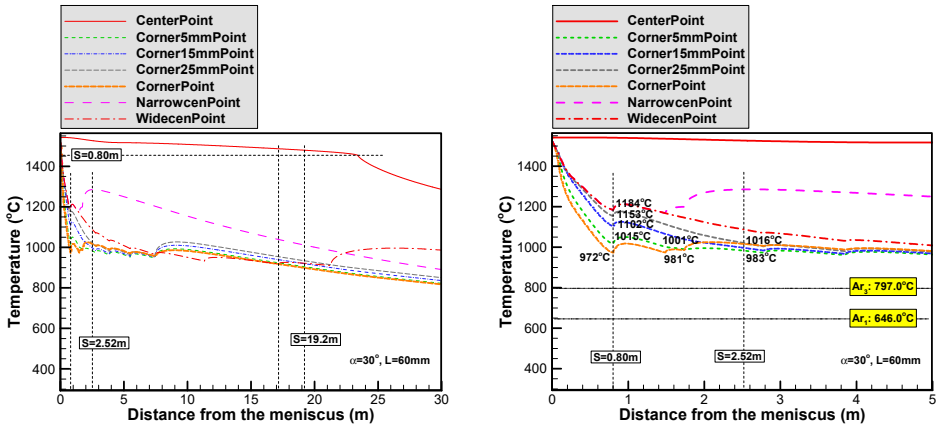

(**a**) (**b**)

Figure 13. Temperature distribution under weak cooling in foot roller zone of the chamfered slab. (**a**) The whole process of slab solidification, (**b**) enlarged view of mould and bending section.

Table 6. Comparation of temperature of chamfered slab under intensive and weak cooling (°C).

Chamfered slab	Intensive Cooling				Weak Cooling			
	CornerPoint	**Corner5mmPoint**	**Corner15mmPoint**	**Corner25mmPoint**	**CornerPoint**	**Corner5mmPoint**	**Corner15mmPoint**	**Corner25mmPoint**
Mould exit (S = 0.8 m)	972	1015	1102	1153	972	1015	1102	1153
Foot roller ending (S = 1.5 m)	791	816	904	964	981	1001	1064	1112
Beginning of bending (S = 2.52 m)	929	891	901	926	1016	983	997	1021
Beginning of straightening (S = 17.16 m)	910	916	931	946	917	924	939	954
Ending of straightening (S = 19.2 m)	891	897	912	891	898	905	920	934

4. Conclusions

(1) The analysis of the metallographic structure of typical micro-alloyed S355 steel shows that the temperature of the slab corner is cooled to that between Ar_3 and Ar_1, such that the ferrite film precipitates along the grain boundary, which causes the grain boundary to become brittle, which is the main reason for the formation of transverse corner cracks of micro-alloyed steel during the bending and straightening processes.

(2) The numerical simulation results show that the temperature of the slab corner and its nearby area is quickly reduced to below that of Ar_1 via the intensive cooling method in the foot roller zone of the right-angle slab. The temperature is returned to the hot ductility trough of S355 at the bending process. The right-angle slab is prone to create transverse corner crack defects during the bending and straightening process, whether under intensive or weak cooling conditions.

(3) Using the chamfered mould technology, during the bending and straightening processes, the temperature of the slab corner is always maintained above that of Ar_3, which avoids harm to the grain boundary ferrite film to the hot ductility of steel. Meanwhile, the embrittlement zone of the steel is also avoided. Transverse corner cracks of the slab can be prevented effectively.

Author Contributions: Conceptualization, M.W. and H.Z.; methodology, M.W., H.Z. and L.X.; software, H.L.; writing—original draft preparation, M.W., H.Z., and H.L.; writing—review and editing, M.W. and H.L.; All authors have read and agreed to the published version of the manuscript.

Funding: This research was funded by National key R&D project of China (No. 2017YFB0304004).

Institutional Review Board Statement: Not applicable.

Informed Consent Statement: Not applicable.

Data Availability Statement: Not applicable.

Conflicts of Interest: The authors declare no conflict of interest.

References

1. Liu, J.; Wen, G.H.; Tang, P. Research status of transversal crack on micro-alloyed steel slab. *J. Iron Steel Res.* **2016**, *28*, 1–9.
2. Lan, P.; Du, C.W.; Chen, P.L.; Liu, H.S.; Qiu, D.S.; Zhang, J.Q. Research status of surface transverse cracking formation mechanism and control technique for continuously cast microalloyed steels. *J. Iron Steel Res.* **2017**, *29*, 1–12.
3. Du, C.W.; Wang, C.L.; Li, B.; Li, B.; Ma, B.C.; Zhang, J.Q. Effect of the temperature field and cooling rate along casting direction surface transverse crack of microalloyed steel. *J. Iron Steel Res.* **2018**, *30*, 523–528.
4. Konishi, J.; Militzer, M.; Brimacombe, J.K.; Samarasekera, I.V. Modeling the formation of longitudinal facial cracks during continuous casting of hypoperitectic steel. *Metall. Mater. Trans. B* **2002**, *33*, 413–423. [CrossRef]
5. Takeuchi, E.; Brimacombe, J.K. Effect of oscillation-mark formation on the surface quality of continuously cast steel slabs. *Metall. Trans. B* **1985**, *16*, 605–625. [CrossRef]
6. Triolet, N.; Poelmans, K.; Mabelly, P.; Le Papillon, Y. Prevention of corner cracks in slab continuous casting. *Rev. Metall.* **2009**, *106*, 508–517. [CrossRef]
7. Tsuprun, A.Y.; Fedosov, A.V.; Pashchuk, D.V.; Tskitishvili, E.O.; Ottsevich, V.V. Reduction in slab surface corner crack damage due to development of rational secondary cooling regimes. *Metallurgist* **2014**, *57*, 824–829. [CrossRef]
8. Mintz, B.; Yue, S.; Jonas, J.J. Hot ductility of steels and its relationship to the problem of transverse cracking during continuous casting. *Int. Mater. Rev.* **1991**, *36*, 187–196. [CrossRef]
9. Zhu, Z.Y.; Zhen, X.G.; Jiang, H.T.; Li, J.G. Control technology of the transverse cracks in 400 mm ultra-thick slabs. *Iron Steel* **2011**, *46*, 33–36.
10. Zeng, Y.N. *Precipitation Mechanism of Second Phase Particles and Control of Surface Cracks in Continuous Casting Slab of Microalloyed Steel*; University of Science and Technology Beijing: Beijing, China, 2014.
11. Ito, Y.; Kato, T.; Yamanaka, A.; Watanabe, T. Improvement of hot ductility in continuously cast strand by ferrite precipitation control. *Tetsu-to-Hagan* **2003**, *10*, 1023–1031. [CrossRef]
12. Kato, T.; Ito, Y.; Kawamoto, M.; Yamanaka, A.; Watanabe, T. Prevention of slab surface transverse cracking by microstructure control. *ISIJ Int.* **2003**, *43*, 1742. [CrossRef]
13. Ito, Y.; Murai, T.; Miki, Y.; Mitsuzono, M.; Goto, T. Development of hard secondary cooling by high-pressure water spray in continuous casting. *ISIJ Int.* **2011**, *51*, 1454–1460. [CrossRef]

14. Du, C.; Zhang, J.; Wen, J.; Li, Y.; Lan, P. Hot ductility trough elimination through single cycle of intense cooling and reheating for microalloyed steel casting. *Ironmak. Steelmak.* **2016**, *43*, 331–339. [CrossRef]
15. Cai, Z.Z.; An, J.Z.; Liu, Z.Y.; Niu, Z.Y.; Zhu, M.Y. Development and application of micro-alloyed steel slab corner transversal crack control technology. *J. Iron Steel Res.* **2019**, *31*, 117–124.
16. Wang, M.L.; Yang, C.Z.; Tao, H.B.; Zhang, H.; Liu, J.H.; Wu, Y.M. Formation mechanism of transverse corner crack on micro-alloyed steel slab. *Iron Steel* **2012**, *47*, 27–33, 39.
17. Cao, J.X.; Tao, H.B.; Zhang, H.; Zhou, M.W.; Zhang, L.Z.; Peng, M.Y. Application of chamfered mould on slab continuous casting production in Lianyuan iron and steel company. *Iron Steel* **2013**, *48*, 43–47.
18. Ren, F.F.; Zhang, H.; Wang, W.N.; Wang, M.L. Numerical simulation of actual temperature field for chamfered mold copper. *Iron Steel* **2015**, *50*, 27–33.
19. Yang, X.S.; Zhang, P. Development and application of chamfered mold technology. *Contin. Cast.* **2018**, *43*, 26–31.
20. Liu, G.L.; Liu, Q.; Ji, C.X.; Chen, B.; Li, H.B.; Liu, K. Application of a novel chamfered mold to suppress corner transverse cracking of micro-alloyed steel slabs. *Metals* **2020**, *10*, 1289. [CrossRef]
21. Muzumdar, D. A consideration about the concept of effective thermal conductivity in continuous casting. *ISIJ Int.* **1989**, *29*, 524–528. [CrossRef]
22. Choudhary, S.K.; Mazumdar, D.; Ghosh, A. Mathematical modeling of heat transfer phenomena in continuous casting of steel. *ISIJ Int.* **1993**, *33*, 764–774. [CrossRef]
23. Tieu, A.K.; Kim, I.S. Simulation of the continuous casting process by a mathematic model. *Int. J. Mech. Sci.* **1997**, *39*, 185–192. [CrossRef]
24. Hardin, R.A.; Liu, K.; Kapoor, A.; Beckermann, C. A transient simulation and dynamic spray cooling control model for continuous steel casting. *Metall. Mater. Trans. B* **2003**, *34*, 297–306. [CrossRef]